American Mineralogist, Volume 66, pages 324-333, 1981

High-pressure crystal structure and compressibility of coesite

LOUISE LEVIEN[1] AND CHARLES T. PREWITT

Department of Earth and Space Sciences
State University of New York
Stony Brook, New York 11794

Abstract

Unit-cell and crystal-structure parameters have been measured on a coesite single crystal at six pressures. Unit-cell parameters of coesite change from $a = 7.1356(3)$, $b = 12.3692(8)$, $c = 7.1736(3)$Å and $\beta = 120.34(02)°$ at 1 atm to $a = 6.9897(4)$, $b = 12.233(2)$, $c = 7.1112(4)$ Å and $\beta = 120.74(03)°$ at 51.9 kbar. Both silicate tetrahedra compress significantly but do not distort over the 52 kbar pressure range. All unconstrained Si–O–Si angles and Si···Si distances decrease over the pressure range, with smaller angles and distances decreasing more than larger ones. Values for the bulk modulus [$K_T = 0.96(3)$ Mbar] and its pressure derivative [$K'_T = 8.4(1.9)$] have been calculated by fitting the P–V data to a Birch–Murnaghan equation of state. The compressibility of the coesite structure is highly anisotropic with the stiffest direction parallel to the chains of tetrahedra, which run ∥ to c, and the most flexible direction ⊥ to these chains in the a–c plane. The criss-crossing of silicate tetrahedral chains in the a–b planes, at different levels along c, gives b an intermediate compressibility.

The increasing temperature factor of O(1), the central anion in the 180° Si–O–Si angle, suggests that this angle becomes unstable at high pressures. Because substitution of Ge for Si has a similar effect on the structure as does increased pressure, GeO_2 may not exist in the coesite structure because the 180° Ge–O–Ge angle destabilizes the structure.

Introduction

The high-pressure crystal structure of SiO_2 (coesite) has been studied to help us better understand the structural elements which give rise to its single-crystal elastic moduli and to permit a comparison between coesite and SiO_2 (quartz), the low-pressure polymorph. We felt that investigations of these two silica polymorphs, because of their simple chemistry, would increase our understanding of the changes that silicate tetrahedra undergo at high pressure, and we would thus better understand the behavior of all silicates under pressure. We also hoped to gain some insight into why GeO_2 apparently is not stable in the coesite structure.

Experimental techniques

The coesite crystals were synthesized at 65 kbar and 1100°C [this temperature was reported incorrectly as 110°C in Gibbs *et al.* (1977)]. Observations made under the optical microscope and with precession and Weissenberg X-ray photographs showed the crystals to be untwinned. Crystal #1 was an elongated hexagonal plate with dimensions 90 × 60 μm and thickness of 30 μm. Intensity data were collected on this crystal at ambient conditions and two high pressures. Refinements of the high-pressure data gave reasonable R values, but very large errors on positional parameters; in addition, structural parameters did not show regular changes as a function of pressure. The combination of the small size of the crystal, coupled with the increased background caused by the diamond cell, resulted in very low peak-to-background ratios (42% of intensities were $<2\sigma_I$). A third high-pressure data set, collected with a higher-intensity X-ray beam, gave a refinement with smaller errors on the positional parameters, but the refinement still was not satisfactory. Therefore, we have included the unit-cell data collected on crystal #1 in this report, but not the structural refinements. We next selected a larger crystal (160 × 80 × 60 μm), and collected data until this crystal was broken in the diamond cell during an unsuccessful remounting attempt. The largest remaining fragment (120 × 80 ×

[1] Present address: Exxon Production Research Company, P.O. Box 2189, Houston, Texas, 77001.

0003–004X/81/0304–0324$02.00

60 μm) was used for the two highest-pressure runs (with a noticeable decrease in the quality of the refinements). The diamond-anvil data-collection techniques used for this study were similar to those described by Levien *et al.* (1980) with minor modifications. The Merrill–Bassett (Merrill and Bassett, 1974) cell was used for the highest pressures, whereas a cell with larger diamond faces (1 mm culet) and flat Be discs, like those described by Hazen and Finger (1977), was used to collect the other high-pressure data. All data were collected with Mo$K\alpha$ radiation; a hemisphere of integrated intensities in reciprocal space ($2° < 2\theta < 60°$) was collected on the crystal at room pressure, whereas an entire sphere of intensities $2° < 2\theta < 90°$ (except for reflections affected by diffraction peaks from polycrystalline Be) was collected at each high pressure. Averaging of symmetrically-equivalent reflections gave between 336 and 426 reflections at the high pressures and 783 at 1 atm. From zero to three reflections were rejected from the high-pressure data sets due to obvious overlap with diamond reflections. With the exceptions of five reflections in the isotropic and three in the anisotropic refinements at 1 atm, all observed reflections (greater than $2\sigma_I$) were accepted with the final refinements. An extinction parameter significantly decreased the R values of all six refinements at the 0.005 significance level (Hamilton, 1974); however, not enough data were collected at the high pressures to warrant the increase in the number of parameters (from 25 to 58) to refine anisotropic temperature factors. The final weighted R values of the isotropic refinements ranged from 0.030 to 0.048 (Table 1). Observed and calculated structure factors are listed in Table 2[2]; positional parameters and isotropic temperature factors are given in Table 3; anisotropic temperature factors for the 1-atm refinement are reported in Table 4; interatomic distances and angles for the two silicate tetrahedra are given in Table 5; inter-tetrahedral distances and angles are reported in Table 6; unit-cell parameters are listed in Table 7; and the coefficients and angles that describe the deformation ellipsoid of the unit cell are reported in Table 8.

Table 1. Intensity information for coesite at six pressures

	total #data	#after av.*	$\#>2\sigma_I$**	wR	R	Ext. X 10^{-4}†
1 atm iso	838	783	742	0.048	0.028	0.42(4)††
1 atm aniso	838	783	742	0.030	0.017	0.42(2)
21.8 kbar	1016	336	260	0.039	0.041	0.31(4)
31.5 kbar	993	342	266	0.039	0.045	0.36(4)
38.7 kbar	1008	346	264	0.039	0.045	0.32(4)
46.0 kbar	1037	426	303	0.040	0.053	0.19(2)
51.9 kbar	993	391	274	0.040	0.055	0.20(3)

**Number of data after symmetrically equivalent reflections were averaged.*
***Number of data accepted in the refinement. All were greater than $2\sigma_I$.*
†Refined secondary extinction parameters.
††Parenthesized figures represent esd's of least units cited.

Results

Although some of the positional parameters from the previous refinement of the crystal structure of coesite (Gibbs *et al.*, 1977) are significantly different from those determined here, the Si–O bond distances are essentially identical. All the equivalent isotropic temperature factors in Gibbs *et al.* are larger than those determined in our study. This may be due to the fact that no crystal X-ray absorption correction was applied to their data before an extinction parameter was refined (Baldwin, personal communication). Both corrections were made in our refinement. In both refinements the weighted R values are considerably larger than the unweighted values, suggesting that in both cases the strong reflections (which have smaller relative sigmas) show more scatter than the data set as a whole. We see no evidence in the refinements at high pressures for a phase change to a structure like that reported by Kirfe *et al.* (1979).

The unit cell for monoclinic coesite is nearly pseudohexagonal at room pressure with a and c approximately equal and $\beta = 120.34°$; however, changes in the cell with increased pressure cause it to appear less hexagonal. The a direction compresses more than twice as much as the c direction, with a changing 0.1459Å in 52 kbar and c changing only 0.0624Å. In addition, the β angle increases to 120.74°.

The strain ellipsoids (Ohashi and Burnham, 1973), which describe the deformation of the unit cell, have been calculated for the pressure range studied, and the principal axes and their orientations for crystal #2 are reported in Table 8. For coesite, the directions of minimum and maximum compression both lie in the a–c plane, with the minimum compression direction $\parallel$ to c, and the maximum compression direction 90° away ($\parallel$ to a^*). The symmetry axis, b, is parallel to the intermediate axis. The orientation of this ellipsoid does not change with pressure. The stiffness along c increases very little with increased pressure, whereas the stiffness along b, the intermediate direc-

[2] To receive a copy of Table 2, order document AM-81-150 from the Business Office, Mineralogical Society of America, 2000 Florida Avenue, N.W., Washington, D.C. 20009. Please remit $1.00 in advance for the microfiche.

Table 3. Positional and thermal parameters of coesite at pressure

		1 atm iso	1 atm aniso	21.8*	31.5	38.7	46.0	51.9
Si(1)	x	0.14033(7)**	0.14035(5)	0.1385(1)	0.1378(1)	0.1374(1)	0.1370(1)	0.1369(2)
	y	0.10833(3)	0.10833(2)	0.1089(3)	0.1093(3)	0.1095(3)	0.1098(3)	0.1101(3)
	z	0.07227(8)	0.07230(5)	0.0714(1)	0.0711(1)	0.0707(1)	0.0704(2)	0.0704(2)
	B	0.41(2)	0.42(1)	0.42(2)	0.44(2)	0.40(2)	0.38(2)	0.41(2)
Si(2)	x	0.50682(7)	0.50674(5)	0.5078(1)	0.5081(1)	0.5085(1)	0.5085(2)	0.5087(2)
	y	0.15799(4)	0.15796(2)	0.1578(2)	0.1576(2)	0.1572(2)	0.1576(3)	0.1574(3)
	z	0.54077(7)	0.54072(4)	0.5426(1)	0.5434(1)	0.5439(1)	0.5441(2)	0.5446(2)
	B	0.40(2)	0.42(1)	0.41(2)	0.43(2)	0.38(2)	0.35(2)	0.38(2)
O(1)†	B	0.71(3)	0.71(2)	0.90(6)	0.91(5)	0.90(6)	1.03(7)	0.94(7)
O(2)††	y	0.1163(1)	0.11634(9)	0.1124(8)	0.1107(8)	0.1095(8)	0.1091(8)	0.1085(9)
	B	0.68(3)	0.70(2)	0.64(5)	0.69(5)	0.55(5)	0.64(6)	0.55(6)
O(3)	x	0.2660(2)	0.2661 (1)	0.2605(4)	0.2576(4)	0.2558(4)	0.2543(4)	0.2540(5)
	y	0.1234(1)	0.12324(7)	0.1259(6)	0.1272(6)	0.1279(6)	0.1291(5)	0.1298(6)
	z	0.9401(2)	0.9401 (1)	0.9346(4)	0.9320(4)	0.9302(4)	0.9284(4)	0.9282(5)
	B	0.79(2)	0.79(1)	0.66(3)	0.67(3)	0.62(3)	0.57(4)	0.62(4)
O(4)	x	0.3114(2)	0.3114 (1)	0.3144(4)	0.3157(4)	0.3167(4)	0.3179(4)	0.3187(5)
	y	0.1038(1)	0.10378(7)	0.1020(6)	0.1020(6)	0.1006(6)	0.1006(6)	0.1005(6)
	z	0.3282(2)	0.3280 (1)	0.3266(4)	0.3263(4)	0.3257(4)	0.3251(4)	0.3251(5)
	B	0.81(2)	0.85(2)	0.76(4)	0.76(4)	0.73(4)	0.74(4)	0.74(5)
O(5)	x	0.0172(2)	0.0175 (1)	0.0217(4)	0.0234(4)	0.0246(4)	0.0264(5)	0.0275(5)
	y	0.2117(1)	0.21177(7)	0.2123(6)	0.2126(6)	0.2135(6)	0.2129(6)	0.2126(7)
	z	0.4782(2)	0.4784 (1)	0.4745(4)	0.4728(4)	0.4724(4)	0.4719(5)	0.4714(5)
	B	0.75(2)	0.76(2)	0.82(4)	0.82(4)	0.79(4)	0.80(5)	0.80(5)

* *Pressures are reported in kbar unless otherwise indicated.*
** *Parenthesized figures represent esd's of least units cited.*
† *The positional parameters for O(1) are (0, 0, 0).*
†† *The x and z positional parameters for O(2) are 0.5 and 0.75, respectively.*

tion, becomes almost as great as that along c by the 46.0–51.9 kbar range.

The two symmetrically-distinct silicate tetrahedra in coesite respond differently to increased pressure. In the Si(1) tetrahedron, two Si–O bonds [the longest, Si(1)–O(5), and one intermediate in length, Si(1)–O(3)] stay approximately the same, whereas the shortest and the other intermediate bond, Si(1)–O(1) and Si(1)–O(4), compress significantly (Table 5). From a standard deviation of the mean Si–O distance, calculated by propagation of errors, the average bond length can be said to shorten significantly. Other evidence that supports this claim is that a significant decrease in tetrahedral volume occurs, from 2.138 to 2.110Å^3, (Table 5) with estimated errors on these values no larger than 0.003Å^3. The quadratic elongation (Robinson *et al.*, 1971) of the Si(1) tetrahedron does not change over the pressure range, and therefore the volume change cannot be accounted for by polyhedral distortion and must be a result of the compression of Si–O bonds. Of the internal tetrahedral angles, the largest change is observed in the O(1)–Si(1)–O(4) angle, changing from 109.32(5)° to 107.4(3)°. Coincident with this change is the largest change in tetrahedral O–O distances [between O(1) and O(4)], from 2.616(1) at 1 atm to 2.560(7)Å at 51.9 kbar. These are also the two oxygens that form the compressible Si–O bonds in the Si(1) tetrahedron.

The Si(2) tetrahedron also changes anisotropically so that all four Si(2)–O bonds compress, but with only the longest two, Si(2)–O(3) and Si(2)–O(5), changing significantly (Table 5). When the standard deviation of the mean Si(2)–O distance is calculated

Table 4. Anisotropic temperature factors for coesite at 1 atm

	β_{11}*	β_{22}	β_{33}	β_{12}	β_{13}	β_{23}
Si(1)	30. (1)**	6.5(3)	28.(1)	-2.8(2)	15.2(8)	-1.9(2)
Si(2)	32.9(9)	7.4(3)	24.(1)	-1.1(2)	16.0(7)	-0.8(2)
O(1)	50. (3)	6.4(7)	56.(3)	-6. (1)	22. (2)	-3. (1)
O(2)	66. (3)	12.1(7)	35.(3)	0.	34. (2)	0.
O(3)	50. (2)	16.0(5)	55.(2)	-4.8(8)	37. (2)	-2.4(8)
O(4)	60. (2)	15.2(6)	31.(2)	-6.3(7)	11. (2)	-4.6(7)
O(5)	53. (2)	7.7(5)	68.(2)	-0.1(7)	33. (2)	1.5(8)

* *All β's are given X 10^4.*
** *Parenthesized figures represent esd's of least units cited.*

Table 5. Tetrahedral distances and angles of coesite at pressure

	1 atm iso	1 atm aniso	21.8*	31.5	38.7	46.0	51.9
Intra-tetrahedral distances (Å)							
Si(1)-O(1)	1.5945(4)**	1.5946(3)	1.583(3)	1.581(3)	1.578(3)	1.578(3)	1.578(3)
Si(1)-O(3)	1.611 (1)	1.6118(9)	1.612(3)	1.611(3)	1.610(3)	1.613(3)	1.611(3)
Si(1)-O(4)	1.612 (1)	1.6113(9)	1.605(4)	1.603(5)	1.603(4)	1.600(6)	1.599(5)
Si(1)-O(5)	1.619 (1)	1.6197(8)	1.623(7)	1.623(6)	1.631(7)	1.625(7)	1.622(7)
<Si(1)-O>	1.6092(6)	1.6094(4)	1.606(2)	1.604(2)	1.606(2)	1.604(3)	1.603(2)
Intra-tetrahedral angles (deg)							
O(1)-Si(1)-O(3)	110.52(6)	110.46(4)	110.4(2)	110.2(2)	110.2(2)	110.3(2)	110.4(2)
O(1)-Si(1)-O(4)	109.32(5)	109.34(3)	108.5(3)	108.3(3)	107.7(3)	107.5(3)	107.4(3)
O(1)-Si(1)-O(5)	109.89(5)	109.85(3)	110.2(2)	110.3(2)	110.5(2)	110.3(2)	110.1(2)
O(3)-Si(1)-O(4)	110.32(7)	110.32(5)	110.6(1)	110.9(1)	111.0(1)	111.0(1)	110.9(1)
O(3)-Si(1)-O(5)	107.89(7)	107.94(5)	108.0(3)	108.0(3)	107.7(3)	107.8(3)	108.0(3)
O(4)-Si(1)-O(5)	108.87(7)	108.91(5)	109.2(2)	109.1(3)	109.7(3)	109.9(3)	110.0(3)
Intra-tetrahedral distances (Å)							
O(1)-O(3)	2.634(1)	2.6339(8)	2.624(5)	2.619(5)	2.615(5)	2.619(5)	2.619(5)
O(1)-O(4)	2.616(1)	2.6154(8)	2.587(5)	2.581(8)	2.569(7)	2.563(8)	2.560(7)
O(1)-O(5)	2.630(1)	2.6306(8)	2.629(8)	2.629(7)	2.637(8)	2.628(8)	2.623(8)
O(3)-O(4)	2.646(2)	2.645 (1)	2.645(3)	2.646(4)	2.648(4)	2.647(4)	2.645(4)
O(3)-O(5)	2.611(2)	2.613 (1)	2.617(5)	2.616(5)	2.617(5)	2.617(5)	2.616(5)
O(4)-O(5)	2.628(2)	2.629 (1)	2.632(7)	2.628(9)	2.644(8)	2.640(9)	2.639(8)
<O-O>	2.628	2.628	2.622	2.620	2.622	2.619	2.617
Quad. Elong.	1.0003	1.0002	1.0004	1.0005	1.0007	1.0007	1.0007
Tetra. Vol.(Å^3)	2.138	2.138	2.124	2.118	2.122	2.115	2.111
Intra-tetrahedral distances (Å)							
Si(2)-O(4)	1.604 (1)	1.6035(9)	1.606(5)	1.601(6)	1.606(5)	1.604(6)	1.601(6)
Si(2)-O(2)	1.6109(7)	1.6106(5)	1.611(4)	1.610(4)	1.609(4)	1.611(4)	1.608(4)
Si(2)-O(3)	1.614 (1)	1.6144(8)	1.610(3)	1.611(3)	1.610(3)	1.609(3)	1.604(4)
Si(2)-O(5)	1.619 (1)	1.6190(9)	1.609(8)	1.606(7)	1.598(7)	1.600(7)	1.606(8)
<Si(2)-O>	1.6118(6)	1.6119(4)	1.609(3)	1.607(3)	1.606(2)	1.606(3)	1.605(3)
Intra-tetrahedral angles (deg)							
O(4)-Si(2)-O(2)	109.35(6)	109.43(4)	109.0(3)	109.0(3)	108.9(3)	109.0(3)	109.0(3)
O(4)-Si(2)-O(3)	108.85(7)	108.83(5)	108.6(3)	108.8(3)	108.8(3)	108.6(3)	108.5(3)
O(4)-Si(2)-O(5)	109.38(7)	109.34(4)	109.7(3)	109.6(3)	109.8(3)	109.9(3)	109.8(3)
O(2)-Si(2)-O(3)	109.74(6)	109.69(4)	109.3(2)	109.2(3)	109.1(3)	108.9(3)	109.2(3)
O(2)-Si(2)-O(5)	110.21(8)	110.18(5)	110.5(3)	110.6(3)	110.8(3)	110.8(3)	110.7(4)
O(3)-Si(2)-O(5)	109.30(7)	109.36(4)	109.6(3)	109.5(3)	109.4(3)	109.6(3)	109.4(3)
Intra-tetrahedral distances (Å)							
O(4)-O(2)	2.623(1)	2.6236(8)	2.619(4)	2.615(6)	2.617(4)	2.616(6)	2.614(5)
O(4)-O(3)	2.617(2)	2.617 (1)	2.612(5)	2.612(8)	2.614(6)	2.610(8)	2.602(6)
O(4)-O(5)	2.630(2)	2.629 (1)	2.629(10)	2.620(10)	2.622(10)	2.624(9)	2.625(10)
O(2)-O(3)	2.637(1)	2.6367(8)	2.628(3)	2.626(4)	2.623(3)	2.620(4)	2.619(4)
O(2)-O(5)	2.649(2)	2.648 (1)	2.646(11)	2.645(11)	2.640(11)	2.643(11)	2.645(11)
O(3)-O(5)	2.637(2)	2.638 (1)	2.630(9)	2.627(9)	2.619(9)	2.621(8)	2.621(9)
<O-O>	2.632	2.632	2.627	2.624	2.622	2.622	2.621
Quad. Elong	1.0001	1.0001	1.0001	1.0001	1.0001	1.0002	1.0002
Tetra. Vol.(Å^3)	2.149	2.149	2.137	2.129	2.125	2.125	2.121

** Pressures are reported in kbar unless otherwise indicated.*
***Parenthesized figures represent esd's of least units cited.*

by propagation of the errors on the individual bonds, the mean Si(2)–O bond length also decreases. Again there is a change in the polyhedral volume (2.149 → 2.121Å^3) and no change in quadratic elongation. The volume decrease must therefore be caused by Si(2)–O bond shortening.

The coesite structure is composed of four-membered rings of silicate tetrahedra linked to form chains ∥ to *c* and in the *a*–*b* plane. Thus, there are five symmetrically-distinct Si–O–Si angles (Table 6, Fig. 1). The smaller angles on this figure seem to be decreasing at a faster rate than the larger ones. The

Table 6. Inter-tetrahedral distances and angles of coesite at pressure

		1 atm iso	1 atm aniso	21.8*	31.5	38.7	46.0	51.9
Inter-tetrahedral angles (deg)								
Si(1)-O(1)-Si(1)	(A)**	180.	180.	180.	180.	180.	180.	180.
Si(2)-O(2)-Si(2)	(B)	142.7 (1)†	142.72(8)	139.4(7)	138.1(7)	137.5(6)	136.7(7)	136.4(7)
Si(2)-O(3)-Si(1)	(C)	144.52(9)	144.45(6)	143.2(2)	142.4(2)	141.8(2)	141.3(2)	141.4(2)
Si(1)-O(4)-Si(2)	(D)	149.64(9)	149.68(6)	149.3(4)	149.6(5)	148.8(5)	148.8(5)	148.8(5)
Si(1)-O(5)-Si(2)	(E)	137.36(9)	137.29(6)	135.6(2)	134.8(2)	134.5(2)	133.6(2)	132.9(3)
Inter-tetrahedral distances (Å)								
Si(1)-Si(1)	(A)**	3.1890(9)	3.1892(6)	3.166(6)	3.162(6)	3.157(6)	3.155(6)	3.156(6)
Si(1)-Si(2)	(C)	3.1036(6)	3.1029(4)	3.096(5)	3.091(10)	3.092(7)	3.086(10)	3.082(8)
Si(1)-Si(2)	(D)	3.0720(6)	3.0722(4)	3.057(2)	3.051(3)	3.043(2)	3.040(3)	3.035(2)
Si(1)-Si(2)	(E)	3.0159(6)	3.0164(4)	2.992(4)	2.981(4)	2.978(4)	2.964(4)	2.960(5)
Si(2)-Si(2)	(B)	3.0522(9)	3.0523(5)	3.022(2)	3.008(2)	3.000(2)	2.994(2)	2.986(2)
Inter-tetrahedral distances (Å)								
O(2)-O(4)	(1)††	3.209(2)	3.209(1)	3.116(12)	3.087(12)	3.049(12)	3.034(12)	3.020(13)
O(3)-O(3)	(2)	3.375(3)	3.375(2)	3.264(7)	3.210(11)	3.180(9)	3.147(11)	3.136(9)
O(3)-O(3)	(3)	3.287(3)	3.290(2)	3.219(14)	3.188(14)	3.170(13)	3.143(12)	3.123(13)
O(4)-O(4)	(4)	3.398(3)	3.397(2)	3.317(5)	3.287(5)	3.258(5)	3.230(6)	3.214(6)
O(5)-O(5)	(5)	3.158(2)	3.158(2)	3.064(5)	3.025(5)	3.008(5)	2.987(6)	2.970(6)
O(5)-O(5)	(6)	3.314(2)	3.311(2)	3.196(7)	3.149(7)	3.115(7)	3.085(7)	3.063(8)

Pressures are reported in kbar unless otherwise indicated.
**Letter codes refer to related distances and angles on this table and on Fig. 5.*
†Parenthesized figures represent esd's of least units cited.*
††Number codes are used in the discussion and on Figs. 3 and 4.*

Si(1)–O(1)–Si(1) angle is symmetrically constrained to be 180° and shows the lack of kinking of the chains that run through the *a–b* planes. The Si(2)–O(2)–Si(2) interbond angle shows the largest change, 142.6(1)° → 136.4(7)° and describes the kinking of the chains that run ∥ to *c*. The other three Si–O–Si angles describe distortions within the four-membered rings of tetrahedra. The Si–Si distances (which are related to the Si–O–Si angles) all decrease significantly, again with the smallest distances generally showing the largest changes (Fig. 2). The Si(1)–Si(1) distance can only change from Si(1)–O(1) bond shortening.

The isotropic temperature factors of three of the oxygens change with pressure. That of O(2) decreases slightly and that of O(3) decreases more than twenty percent. The value for O(1) is reasonable at 1 atm, and we therefore agree with Gibbs *et al.* (1977) that O(1) is on a special position, making the Si(1)–O(1)–Si(1) angle 180°, and not an average value as suggested by Liebau (1961). However, the isotropic temperature factor for O(1) increases thirty percent in the pressure range from 0 to 52 kbar, suggesting that the high-pressure structure might be more stable if this angle were less than 180°. The angular deviation from 180° could not, however, be as large as the 20° suggested by Liebau, because a much larger increase in the temperature factor would be required to indicate such a change.

Elasticity

The bulk modulus, K_T, and pressure derivative of the bulk modulus, K'_T, have been calculated by fitting the P–V data (Table 7) to a Birch–Murnaghan equation of state. An unweighted fit gives values of K_T = 0.96(3) Mbar and K'_T = 8.4(1.9); the values for a weighted fit are essentially the same, K_T = 0.96(3) Mbar and K'_T = 8.4(1.6). The agreement of these values with those of other investigators is fair, with published values of K ranging from 0.89 to 1.14 Mbar. Bassett and Barnett (1970) collected P–V data using a tetrahedral press and solid pressure-transmitting medium. By fitting their data to a Birch–Murnaghan equation, they calculated K_T = 1.14 Mbar (using K'_T = 8, which agrees with that of this study). This K_T value may be higher than the others because it was determined under non-hydrostatic conditions. Two ultrasonic studies of polycrystalline coesite by Akimoto (1972) and Liebermann (personal communication) yield values for K_S of 0.93 and 1.05 Mbar, respectively. Finally, K_S = 1.09 Mbar has been calculated from the best model of single-crystal elastic moduli determined by Weidner and Carleton (1977), and K_S = 0.89 Mbar for their alternate model.

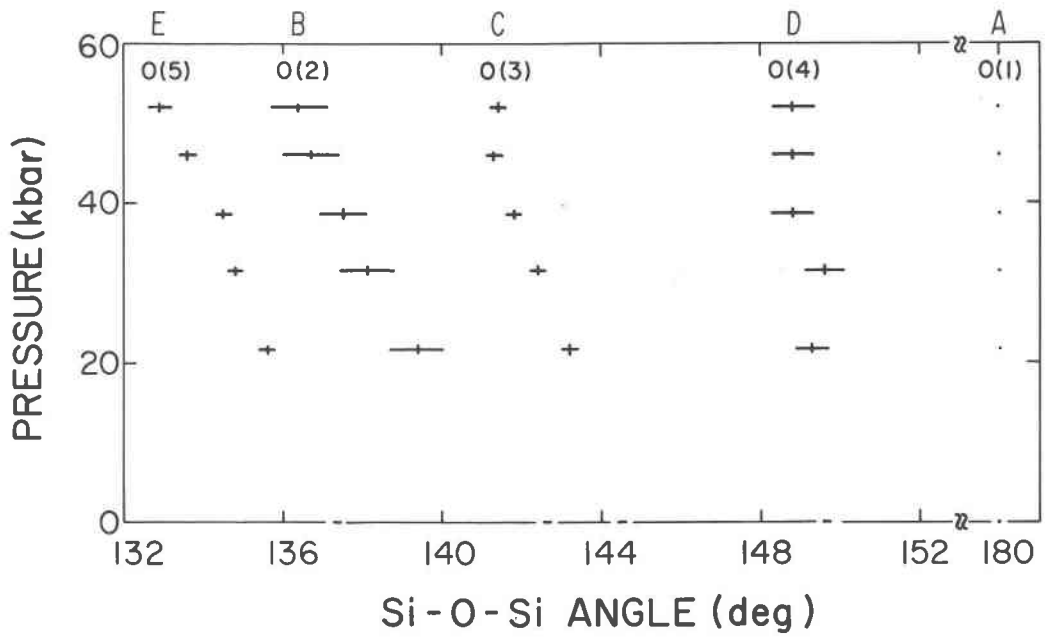

Fig. 1. The five Si–O–Si angles as a function of pressure. Smaller angles change more than larger ones. Letter codes refer to related distances and angles on this figure, Figs. 2 and 5, and Table 6.

We have the most confidence in the K values determined by Weidner and Carleton because they used the single-crystal techniques based on Brillouin scattering spectra. However, because we have performed a careful X-ray diffraction experiment and observed slight imperfections in the crystal used in their study, and because large improvements have been made in these methods of determining elastic moduli since this first crystal was studied, we believe these data may be subject to slightly larger than normal errors. The directions of the principal axes of the strain ellipsoid, which describe the unit-cell deformation, cal-

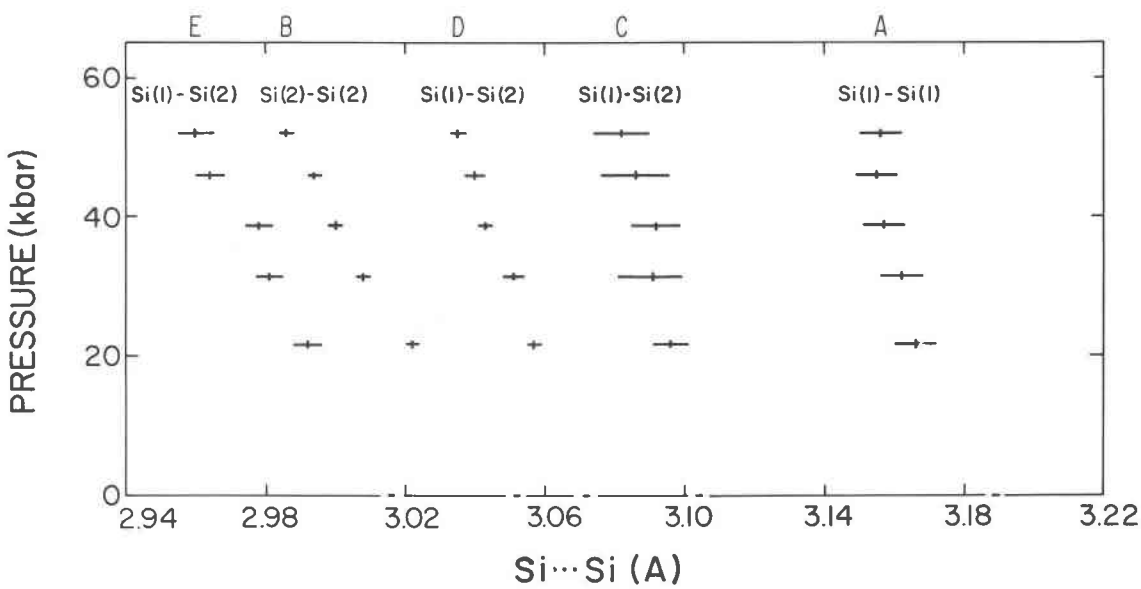

Fig. 2. The five Si···Si distances as a function of pressure. The smaller Si···Si distances change more than the larger ones. The Si(1)–Si(1) distance decreases although the Si(1)–O(1)–Si(1) angle does not. Letter codes refer to related distances and angles on this figure, Figs. 1 and 5, and Table 6.

Table 7. Unit-cell parameters of coesite at pressure

	a (Å)	b (Å)	c (Å)	β (deg)	V (Å^3)
1 atm	7.1356(3)*	12.3692(8)	7.1736(3)	120.34(02)	546.46(5)
21.8(5)**	7.0692(3)	12.306 (1)	7.1462(3)	120.53(02)	535.47(7)
22.4(5)†	7.066 (1)	12.307 (4)	7.145 (1)	120.54(08)	535.1 (2)
31.5(5)	7.0407(5)	12.279 (2)	7.1342(4)	120.61(04)	530.8 (1)
32.4(5)†	7.036 (1)	12.276 (5)	7.132 (1)	120.63(07)	530.0 (2)
38.7(5)	7.0213(2)	12.260 (1)	7.1252(3)	120.66(02)	527.59(6)
40.3(1.)†	7.015 (1)	12.258 (5)	7.1229(8)	120.69(07)	526.6 (2)
46.0(5)	7.0042(5)	12.246 (2)	7.1177(4)	120.70(04)	524.93(9)
51.9(5)	6.9897(4)	12.233 (2)	7.1112(4)	120.74(03)	522.59(9)

*Parenthesized figures represent esd's of least units cited.
**Pressures are reported in kbar unless otherwise indicated.
†Measured on Crystal #1.

culated from Weidner and Carleton's best model of single-crystal elastic moduli, agree within 5° of those calculated from the unit-cell data we determined (Table 8); however, the magnitudes of the changes are different. Our data show the directional compressibilities in the following order $x > y > z$, whereas the order shown by Weidner and Carlton's data is $x > z > y$. Their alternate model agrees with ours in neither direction nor magnitude. We therefore also favor their preferred model; however, we can conclude only that the true value of K is between 0.89 and 1.09 Mbar, and that both sets of P–V data suggest that K'_T is unusually large (~8) for coesite.

The volumes of the silicate tetrahedra that make up the coesite structure account for only 6.3 percent of the unit-cell volume at 1 atm. The change in the volumes of the tetrahedra with pressure accounts for only 1.8 percent of the compression of the unit cell. Therefore, most of the volume change within the structure does not occur within tetrahedral volumes, but between them. There are six O–O pairs that show large decreases in their distances (Table 6); some of these changes are interpreted as closing of channels in the structure. The non-bonded O–O distances have been numbered 1 to 6 for ease of discussion. Distance #1 [O(2)–O(4)] changes 5.9 percent and is very nearly parallel to b (Fig. 3). There are two [O(3)–O(3)] pairs that show large changes: #2 decreases 7.1 percent and #3, 5.0 percent. Number 2 runs nearly parallel to a^* and measures the distance between the chains that run ∥ to c (Fig. 4). Change #3 is not only within a silicate chain, but within one of the groups of four tetrahedra (Fig. 3). The octagonal area around which the four tetrahedra are linked (in the chains that run through the a–b planes) becomes more elongated as pressure increases. Distance #4, [O(4)–O(4)], which decreases 5.4 percent, causes changes similar to those of #3, but in the chains which run parallel to c (Fig. 4). The direction of the change is in the a–c plane rotated approximately 150° from c and 30° from a. The fifth change [O(5)–O(5)] is within a chain and decreases 6.0 percent in the direction ∥ to c (Fig. 4). Change #6 [O(5)–O(5)] is the largest, 7.6 percent, and also indicates the decrease in the distance between chains (Fig. 4) in the a–c plane. Changes #2 and #6 show the largest of the O–O decreases, and both measure the distance across the channels between the silicate chains that run parallel to c. It is not surprising that the a–c plane shows very anisotropic elastic behavior with the strongest direction running parallel to the silicate chains (∥ to c) and the most flexible direction, perpendicular to the chains (∥ to a^*). Why, then, is this anisotropy not observed in the a–b plane, where there are very similar chains that should be more rigid because of their constrained 180° linkages? This pronounced elastic anisotropy is not shown in the a–b plane because the chains run across the unit cell in one direction at the $z = 0$ level [(0,0,0) → (1,1,0)],

Table 8. Principal compression coefficients for coesite at pressure

Pressure range	Principal linear compression coefficients X 10^{-4} per kbar			Volume compression coefficients X 10^{-4} per kbar	Orientations* (deg)		
	ε_1	ε_2	ε_3		ε_1	ε_2	ε_3
1 atm–21.8**	-1.75(3)†	-2.34(5)	-5.15(3)	-9.25(6)	-0.3(3)	b	89.7(3)
21.8-31.5	-1.73(7)	-2.3 (2)	-5.0 (1)	-9.0 (2)	0. (1)	b	90. (1)
31.5-38.7	-1.8 (1)	-2.1 (2)	-4.5 (1)	-8.4 (3)	0. (1)	b	90. (1)
38.7-46.0	-1.4 (1)	-1.6 (2)	-3.9 (1)	-6.9 (3)	2. (2)	b	92. (2)
46.0-51.9	-1.5 (1)	-1.8 (4)	-4.2 (2)	-7.6 (4)	0. (2)	b	90. (2)

*One principal axis is constrained to be || to b. The angles for the other axes are measured from c toward a in (010).
**Pressures are reported in kbar unless otherwise indicated.
†Parenthesized figures represent esd's of least units cited.

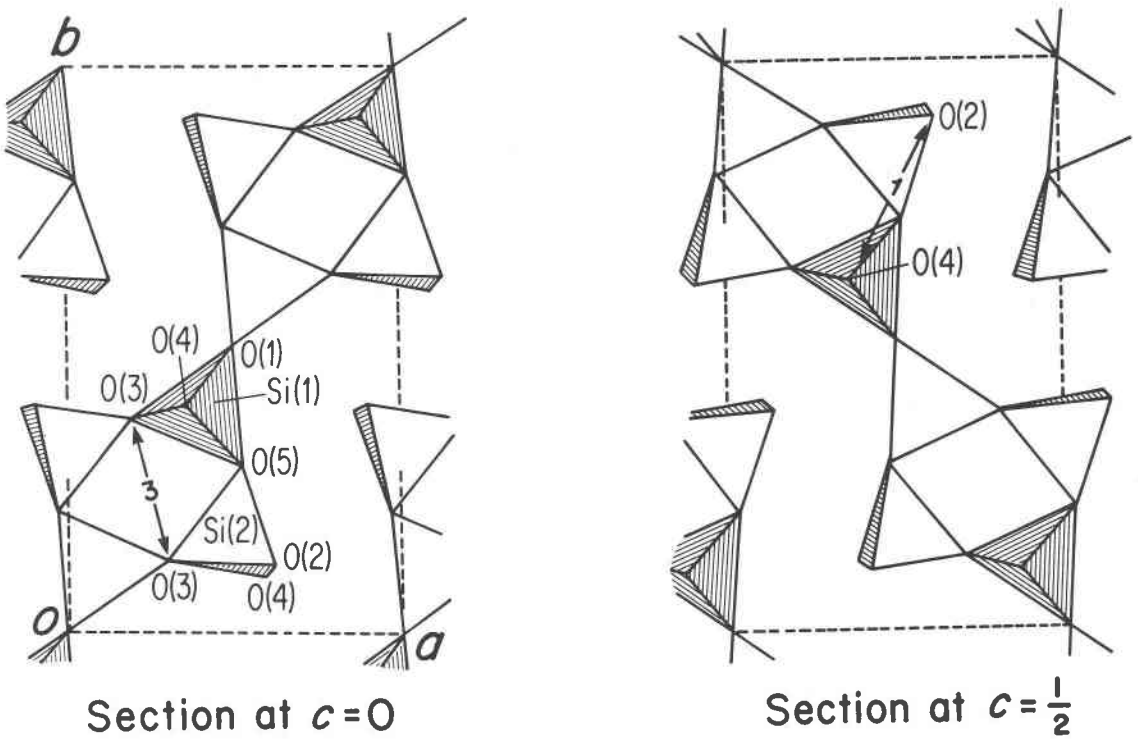

Fig. 3. Projection of crystal structure of coesite parallel to (001) after Zoltai and Buerger, 1959.

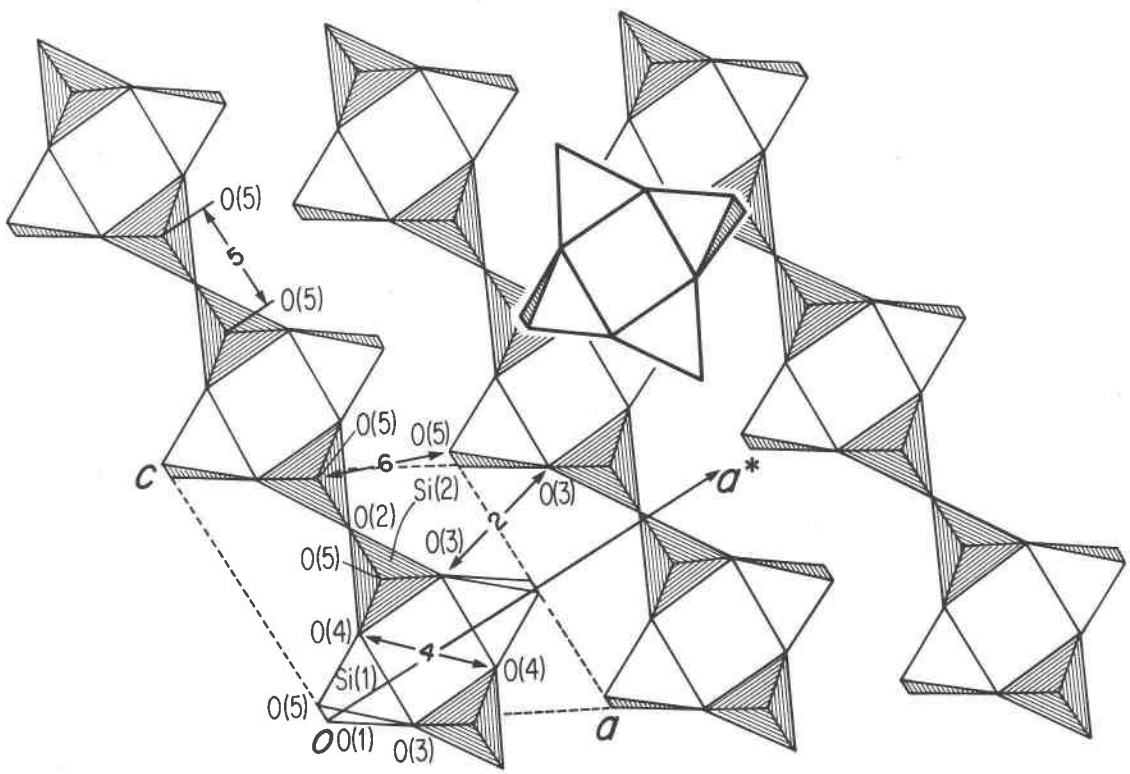

Fig. 4. Projection of crystal structure of coesite parallel to (010) after Zoltai and Buerger, 1959.

and in the other direction at the $z = 0.5$ level [(1,0,0.5) → (0,1,0.5)] (Fig. 3). Because the b axis is longer than the a axis, silicate chains in the a–b plane run at a smaller angle to b than to a. At higher pressures (by the 46 to 52 kbar range), the elastic anisotropy in this plane increases, and the stiffness along b becomes almost as great as that along c. Therefore, the elastic properties of the structure are controlled by rows of silicate chains that are difficult to compress along their lengths, but fairly easy to push together. The cross-hatched pattern of chains in the a–b plane, which does not have as pronounced a grain, gives b an intermediate compressibility.

Discussion

The structures of the two silica polymorphs, quartz (Levien *et al.*, 1980) and coesite, were studied at high pressures to investigate differences in compression of chemically simple and similar minerals. Prior to the experiments, we realized that the bulk moduli of these two minerals were very different. We hypothesized that the tetrahedron in quartz would remain essentially unchanged at high pressure, and that quartz's anomalously large compression would be totally accommodated by its linkages (bond-angle changes). We believed the tetrahedra in coesite were more likely to be deformed with pressure because the linkages were stiffer. The experiments have negated this hypothesis. First, the changes in average Si–O distances between the two structures are not significantly different. Second, Levien *et al.* show that in quartz there are large changes in the internal tetrahedral angles (O–Si–O) that distort the tetrahedron, whereas essentially no distortion takes place in either of the coesite tetrahedra. The largest change in a tetrahedral linkage (Si–O–Si) takes place in quartz (8.6° over 56 kbar); however, large angular changes take place in coesite as well, with the Si(2)–O(2)–Si(2) and Si(1)–O(5)–Si(2) angles changing 6.3° and 4.4°, respectively, over a similar pressure range. Therefore, although the linkages in quartz may be weaker, the tetrahedron in that structure was deformed more by pressure than were those in coesite.

In the SiO_2 system there are three polymorphs as pressure is increased, quartz, coesite, and stishovite, whereas the GeO_2 system has only two (with quartz and stishovite structures). Levien *et al.* (1980) show that in quartz the detailed structural changes that take place with pressure cause it to become more like the room-pressure GeO_2 quartz structure. Our study of the changes that take place in coesite at pressure suggests crystal chemical reasons why GeO_2 (coesite) is not stable. The temperature factor of O(1) increases with pressure, which suggests that the 180° Si(1)–O(1)–Si(1) angle is not stable with increased P. Since substitution of Ge for Si has a similar effect on the structure as increased pressure, this substitution may greatly destabilize the 180° angle and thus the structure. In addition, the GeO_2 (coesite) structure would require a combination of large and small Ge–O–Ge angles that would tend not to be stable.

Hill and Gibbs (1979) report two relationships shown by Si–O–Si angles with d(Si–O) and d(Si···Si) of the silica polymorphs. Levien *et al.* (1980) show that the first relationship sec(Si–O–Si) ∝ d(Si–O) does not hold with increased pressure for quartz, and the coesite data also do not follow this relationship. The regression line of the second relationship (Fig. 5) log sin [(Si–O–Si)/2] ∝ log d(Si···Si) is in much better agreement with the quartz data at pressure. Most of the coesite data also seem to follow a trend near that of the regression line. Of the six sets of angles (five from coesite, one from quartz) plotted on Figure 5, the four angles less than 145° follow approximately the same trend, whereas the two angles larger than 145° follow different trends. O'Keeffe and Hyde

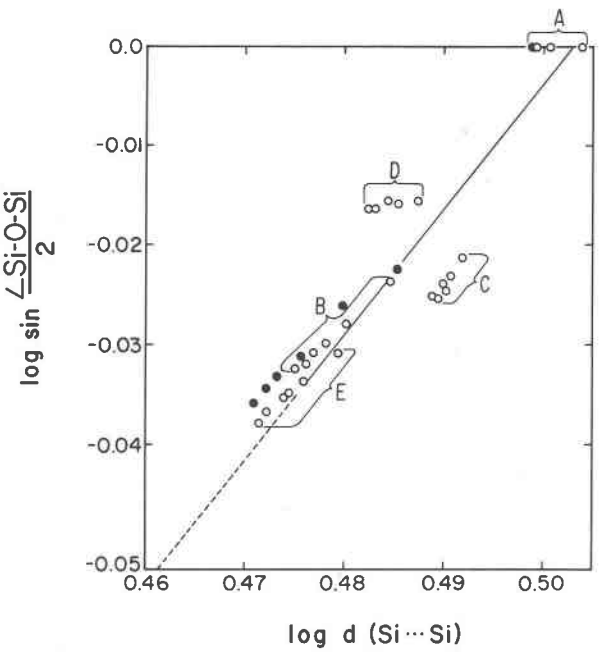

Fig. 5. Plot of log sin [(Si–O–Si)/2] as a function of log d(Si···Si) for the five angles (open circles) in coesite and the one (closed circles) in quartz. The four Si–O–Si angles less than 145° approximate follow the trend shown by all the silica polymorphs at ambient conditions (Hill and Gibbs, 1979). The two angles larger than 145° follow different trends. Letter codes refer to related distances and angles on this figure, Figs. 1 and 2, and Table 6.

(1978) examined the assumption that Si–O–Si angles are controlled by Si···Si contacts and calculated that these contacts exist in Si–O–Si angles less than 145°. The results of our work show that where Si···Si interactions exist, the Si–O–Si angles decrease nearly the same amount per change in Si···Si distance. If additional data on other structures show this trend to hold for structures in general, this relationship may become a powerful tool in the interpretation of structural changes with T and P.

Conclusions

1. Both crystallographically-distinct silicate tetrahedra in coesite compress significantly with increased pressure, but they do not distort.

2. The largest angular changes are generally seen in the smallest Si–O–Si angles (Fig. 1). These changes are coupled with decreasing Si···Si distances, with smaller distances decreasing more than larger ones.

3. There is some scatter in determinations of the bulk modulus for coesite; values we determined are $K_T = 0.96(3)$ Mbar and $K'_T = 8.4(1.9)$. Reliable values of K from several other studies fall between 0.89 and 1.09 Mbar.

4. The compressibility of the coesite structure is highly anisotropic in the a–c plane because of the aligned silicate chains that run parallel to c. The chains are relatively stiff along their lengths, but the structure is relatively flexible in the a^* direction, perpendicular to the chains. This large anisotropy is not observed in the a–b plane, although this plane contains similar silicate chains, because the chains cross each other at different levels along z, causing b to be intermediate in compressibility.

5. Prior to investigating the high-pressure structures of quartz and coesite, we believed that the silicate tetrahedra in quartz were likely to remain rigid, while flexible linkages changed; whereas the tetrahedra in coesite were more likely to distort because the tetrahedral linkages would be stiffer. In fact, despite its more flexible linkages, the quartz tetrahedron distorts more than do those in coesite.

6. If substitution of Ge for Si has the same effect on the structure as high pressure, the 180° Ge–O–Ge angle required in the coesite structure may be unstable, thus precluding GeO_2 (coesite).

7. When log sin [(Si–O–Si)/2] is plotted *vs.* log d (Si···Si), the trend seen for Si–O–Si angles less than 145° seems similar to those shown by all the room-temperature–pressure polymorphs of SiO_2, as described by Hill and Gibbs (1979). The trends for the Si–O–Si angles greater than 145° are different. Because Si···Si interactions are expected to occur in angles of 145° or less (O'Keeffe and Hyde, 1978), nonbonded Si···Si interactions may be important to structural changes that take place with increased temperature or pressure.

Acknowledgments

We thank J. D. Bass for developing the program to calculate the elastic parameters. This research was supported by NSF grant EAR77-13042. The first author also gratefully acknowledges a pre-doctoral fellowship awarded to her by the American Association of University Women Educational Foundation.

References

Akimoto, S.-I. (1972) The system MgO–FeO–SiO_2 at high pressures and temperatures-Phase equilibria and elastic properties. Tectonophysics, 13, 161–187.

Bassett, W. A. and Barnett, J. D. (1970) Isothermal compression of stishovite and coesite up to 85 kilobars at room temperature by X-ray diffraction. Physics of the Earth and Planetary Interiors, 3, 54–60.

Gibbs, G. V., Prewitt, C. T. and Baldwin, K. J. (1977) A study of the structural chemistry of coesite. Zeitschrift für Kristallographie, 145, 108–123.

Hamilton, W. C. (1974) Tests for statistical significance. In J. A. Ibers and W. C. Hamilton, Eds., International Tables for X-Ray Crystallography, Vol. IV, p. 285–310. Kynoch Press, Birmingham, England.

Hazen, R. M. and Finger, L. W. (1977) Modifications in high-pressure single-crystal diamond-cell techniques. Carnegie Institution of Washington Year Book, 76, 655–656.

Hill, R. J. and Gibbs, G. V. (1979) Variation in d(T–O), d(T···T) and ∠TOT in silica and silicate minerals, phosphates and aluminates. Acta Crystallographica, B35, 25–30.

Kirfe, A., Will, G. and Arndt, J. (1979) A new phase of coesite SiO_2. Zeitschrift für Kristallographie, 149, 315–326.

Levien, L., Prewitt, C. T. and Weidner, D. J. (1980) Structure and elastic properties of quartz at pressure. American Mineralogist, 65, 920–930.

Liebau, F. (1961) Untersuchungen über die Grösse des Si–O–Si–Valenzwinkels. Acta Crystallographica, 14, 1103–1109.

Merrill, L. and Bassett, W. A. (1974) Miniature diamond anvil pressure cell for single crystal X-ray diffraction studies. Review of Scientific Instruments, 45, 290–294.

Ohashi, Y. and Burnham, C. W. (1973) Clinopyroxene lattice deformations: The roles of chemical substitution and temperature. American Mineralogist, 58, 843–849.

O'Keeffe, M. and Hyde, B. G. (1978) On Si–O–Si configurations in silicates. Acta Crystallographica, B34, 27–32.

Robinson, K., Gibbs, G. V. and Ribbe, P. H. (1971) Quadratic elongation: a quantitative measure of distortion in coordination polyhedra. Science 172, 567–570.

Weidner, D. J. and Carleton, H. R. (1977) Elasticity of coesite. Journal of Geophysical Research, 82, 1334–1346.

Zoltai, T. and Buerger, M. J. (1959) The crystal structure of coesite, the dense, high-pressure form of silica. Zeitschrift für Kristallographie, 111, 129–141.

Manuscript received, October 17, 1979;
accepted for publication, October 10, 1980.